



# Cutting force modeling and experimental validation for micro end milling

Weijie Wang<sup>1</sup> · Weiwei Zhang<sup>2</sup> · Dingchuan Huang<sup>2</sup> · Wei Wang<sup>2</sup>

Received: 17 December 2020 / Accepted: 26 July 2021 / Published online: 3 August 2021  
© The Author(s), under exclusive licence to Springer-Verlag London Ltd., part of Springer Nature 2021

## Abstract

Micro end milling has an outstanding capability in machining micro-scale structures of various materials. Prediction of cutting forces is significant on controlling quality and safety of machining process. This paper proposes a mechanic model to predict cutting forces in micro end milling process, which includes a novel algorithm of instant uncut chip thickness. This algorithm takes into account the geometric errors of machining system and trochoidal trajectory of cutting edge, which redefines cutting radii with consideration of the tool runout. A feasible technique to reduce the influence of tool runout is put forward by analyzing the redefined cutting radii. Since the existing method for cutting force coefficient identification is generally conducted using finite element simulation, it is difficult for some composite materials due to lack of the material properties. To overcome the above shortcomings, an experimental-based cutting force coefficient identification technique has been developed by groove milling. A number of experimental testing have been conducted to validate the developed cutting force model. Experimental results are in good agreement with theoretical predictions, which demonstrates the validity of proposed cutting force modeling.

**Keywords** Cutting force · Micro end milling · Tool runout · Mechanic model · Chip thickness

## 1 Introduction

The world market of micro-scale products grows with a speed of over 20% every year, a number of micro-components with a dimension ranging from 0.1 to 10 mm and feature dimension from 1  $\mu\text{m}$  to 1 mm came into application [1], most notably in the industries of electronics and biomedical [2]. These micro-components are made of a variety of materials including metallic alloys, ceramics, and polymers. Among all the micro-fabrication methods, micro-milling is one of the most promising techniques for its outstanding machinability for a wide range of materials [3, 4]. Besides, compared to lithography, laser machining, and micro-electro-mechanical systems,

micro-milling is capable of complex 3D structure fabrication [5].

In micro-milling process, the diameter of cutting tools varies from 0.05 to 1 mm [6]. With the decreasing of cutting tool's diameter, the cutting tool rigidity reduces, and it is easier to break. Due to the limitations of cutting tool manufacturing technology, blunt radius cannot be reduced proportionally with the diameter decreasing, which makes micro-milling process different from macro-milling. Blunt radius of micro-milling tool usually ranges from 0.5 to 5  $\mu\text{m}$ , which is similar to the range of feed per tooth. Therefore, cutting edge is not considered as absolutely sharp in micro end milling, and issues including minimum chip thickness, tool runout effect, and plowing effect occur [7]. As a manifestation of size effect, cutting force model is vital to optimize micro-milling process.

Tansel et al. found that the static force in the feed direction of micro end milling was a simple and reliable indicator of tool condition monitoring, including tool wear and cutting edge-damage, and thus proposed two methods for estimation of the static cutting force [8]. Bao and Tansel developed an analytical cutting force model to predict cutting force in micro end milling. The instant uncut chip thickness was calculated by considering cutting edge as a trochoidal trajectory [9]. However, tool runout was not considered in the proposed

✉ Weiwei Zhang  
zhangweiwei0509103@163.com

Weijie Wang  
wangweijie@tju.edu.cn

<sup>1</sup> Key Laboratory of Mechanism Theory and Equipment Design of Ministry of Education, Tianjin University, Tianjin 300072, China

<sup>2</sup> Institute of Electronic Engineering, China Academy of Engineering Physics, Mianyang 621900, China

model. Further, the uncut chip thickness model was modified with consideration of tool runout. The tool runout can be estimated from experimental cutting force data [10]. Li et al. proposed a new model for determining the undeformed chip thickness in micro-milling [11]. The method was based on a true tooth path and using a Taylor's series rather than numerical method for theoretical analysis. Dow et al. established a force model and calculated tool deflection [12]. The proposed model includes cutting force on rake face and friction on the flank face. Vogler et al. developed a cutting force model by considering the minimum chip thickness effect [13]. Cutting coefficients were obtained using finite element (FE) simulation. Bissacco et al. obtained the cutting coefficients by analytical expressions and proposed cutting force model [14]. Lai et al. modified a Johnson-Cook constitutive equation to model material strengthening behaviors [15]. An analytical model was developed based on FE simulation using slip-line theory. Malekian and Park identified cutting coefficients by a nonlinear curve fitting with minimized error through a steepest descent algorithm, and plastic recovery was included in the proposed model [16]. Jin et al. obtained the cutting coefficients based on FE simulation result [17]. In the proposed model, cutting coefficients were expressed as an exponential function of uncut chip thickness and cutting edge radius. Predicted cutting force well coincides with experimental data in the normal direction but less accurately in the feed direction. Jing et al. used a hybrid approach to develop a force model [18]. Cutting coefficients were obtained based on FE simulation. De oliveira et al. studies the size effect in different milling scales and found that size effect exists in both macro- and micro-milling [19]. The minimum uncut chip thickness varied approximately between 1/4 and 1/3 of tool edge radius. Grossi et al. studied cutting coefficient in milling operations and found it changes appreciably with spindle speed [20]. Mamedov et al. put forward a new model by considering tool deflection, but tool runout was not considered [21]. Thepsonthi et al. predicted cutting force totally based on FE simulation, but it is hard to set up a model of real tools due to different machining technology [22]. Zhang et al. established an accurate geometric model of instant uncut chip thickness for both plowing domain and shearing domain, and based on the geometric model, the error between predicted and experimental forces was below 16% [23]. Yuan et al. proposed a force model and discussed the influence of tool runout on cutting force. Single-edge-cutting phenomenon occurred when tool runout increases [24, 25]. Zhou et al. discussed tool runout effect in different situations and established an uncut chip thickness model and observed that elastic recovery has significant effect on cutting force at a low feed speed [26]. Zhang et al. modeled cutting force in micro flat end milling process and by considering tool runout and tilt deviation [27]. The influence of bottom edge effect can be significant when axial depth is small.

In most research, the cutting force model combined both analytical method and FE simulation. FE simulation was often used to obtain cutting force coefficients. Micro end milling is promising for its machinability of variety materials, but FE simulation is limited by its finite material library. Besides, a precise FE model of cutting tool is unreachable due to complex manufacturing technology of cutting tools. Blunt radius is discrepant even for the same series of cutting tools, and different coating layers behave differently in milling process. The minimum uncut chip thickness in above models was mainly estimated in an orthogonal FE simulation instead of experimental operation, which demands a higher accuracy of FE model. Some researchers calculate cutting coefficients with an analytic expression. However, tool geometric parameters still need to be measured with various instruments. There is also another way to obtain cutting coefficients by conducting orthogonal cutting experiments, which are costly and time-consuming for new combination of tools and materials.

In order to overcome limitation of current research, a new cutting force model is developed in micro end milling, which obtains cutting force coefficients using milling experiment instead of FE simulation and orthogonal cutting experiment. The proposed model is developed based on mechanistic model presented by Armarego, which is used to predict macro-milling force. The mechanistic model is adapted to micro end milling by taking tool runout and trochoid trajectory into account. A new method is proposed to measure tool runout precisely. The approach proposed in this paper can be easily extended to any milling process and estimate cutting force rapidly without huge amount of calculation.

This paper is organized as follows: Sect. 2 describes algorithm for calculating cutting coefficients and the mechanistic model of micro-milling force by consideration of tool runout. Section 3 shows the details of experiment setup and cutting parameters. Results are presented and discussed in Sect. 4 and followed by conclusions in Sect. 5.

## 2 Cutting force model

The cutting force model is based on the conventional generic mechanics of cutting approach theory proposed by Armarego [28]. The instantaneous tangential and radial components of cutting force are proportional to the cutting area. The cutting force model below takes the tool runout into consideration and utilizes a new way to predict cutting force coefficients based on experiment in specific cutting conditions.

### 2.1 Mechanical model of cutting force

During micro end milling, there exist two different material removal mechanisms, plowing effect and shear effect.

Plowing effect is negligible when the feed per tooth is twice larger than minimum chip thickness. Thus, cutting force can be predicted in several specific cutting conditions without consideration of plowing effect. The general slot end milling process is shown in Fig. 1. The  $x$  axis and  $y$  axis are opposite to feed direction and cross the feed direction, respectively. To model cutting forces, the cutting tool is segmented into a number of elements along  $z$  axis with equal thickness  $dz$ ; each element can be considered as an oblique cutting with an inclination angle equal to helix angle. Cutting force components of each element can be expressed by:

$$\begin{cases} dF_{t_j}(\theta) = [K_{te} + K_{tc}h(\theta)]dz \\ dF_{r_j}(\theta) = [K_{re} + K_{rc}h(\theta)]dz \\ dF_{a_j}(\theta) = [K_{ae} + K_{ac}h(\theta)]dz \end{cases} \quad (1)$$

where  $dF_{t_j}(\theta)$ ,  $dF_{r_j}(\theta)$ ,  $dF_{a_j}(\theta)$  represent the tangential, radial, and axial cutting force component at the rotation angle  $\theta$  of  $j$ th cutting edge.  $K_{tc}$ ,  $K_{rc}$ , and  $K_{ac}$  are the cutting force coefficients in tangential, radial, and axial directions, respectively.  $K_{te}$ ,  $K_{re}$ , and  $K_{ae}$  are the edge force coefficients in tangential, radial, and axial directions, respectively.  $h(\theta)$  denotes the instantaneous uncut chip thickness at rotation angle  $\theta$ .  $\theta$  is measured clockwise from positive  $y$  axis relative to  $j$ th cutting edge. The rotation angle of element at axial location  $z$  of  $j$ th cutting edge can be expressed as  $\theta_{jz} = \theta + 2j\pi/N_0 - R \cdot z \cdot \tan\beta$ , where  $N_0$  is the number of cutting edges and  $\beta$  and  $R$  are helix angle and radius of cutting tool, respectively.

To transform cutting force components into milling coordinate,  $dF_{t_j}(\theta, z)$  and  $dF_{r_j}(\theta, z)$  are decomposed along  $x$  axis and  $y$  axis and added, which is shown as follows:

$$\begin{cases} dF_x = -dF_t \cos(\theta) - dF_r \sin(\theta) \\ dF_y = dF_t \sin(\theta) - dF_r \cos(\theta) \end{cases} \quad (2)$$

As shown in Fig. 2, due to existence of helix angle, the height of element along axial direction can be expressed as:

$$dz = \frac{Rd\theta}{\tan\beta} \quad (3)$$

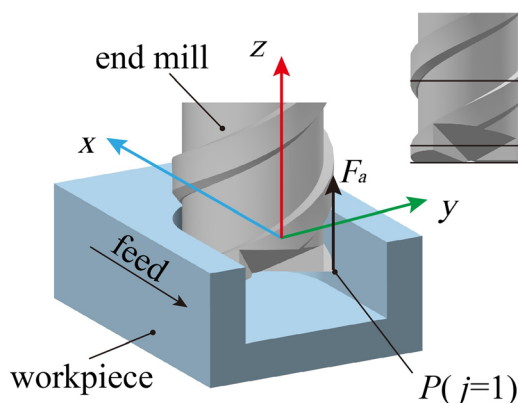


Fig. 1 General slot milling process

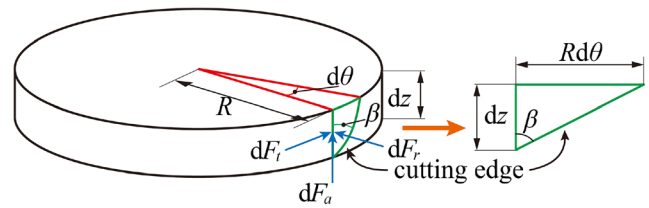


Fig. 2 Relationship between  $dz$  and  $\theta$  in cutting tool element

where  $R$  and  $d\theta$  represent actual cutting radius and the radius of cutting edge’s projection on end face and  $\beta$  is helix angle of cutting tools.

Substituting Eqs. (3) and (2) into Eq. (1), the following equation can be obtained:

$$\begin{cases} dF_x(\theta) = (-K_{tc}h(\theta) + K_{te})\cos(\theta) - (K_{rc}h(\theta) + K_{re})\sin(\theta) \frac{Rd\theta}{\tan\beta} \\ dF_y(\theta) = ((K_{tc}h(\theta) + K_{te})\sin(\theta) - (K_{rc}h(\theta) + K_{re})\cos(\theta)) \frac{Rd\theta}{\tan\beta} \\ dF_a(\theta) = (K_{ae} + K_{ac}h(\theta)) \frac{Rd\theta}{\tan\beta} \end{cases} \quad (4)$$

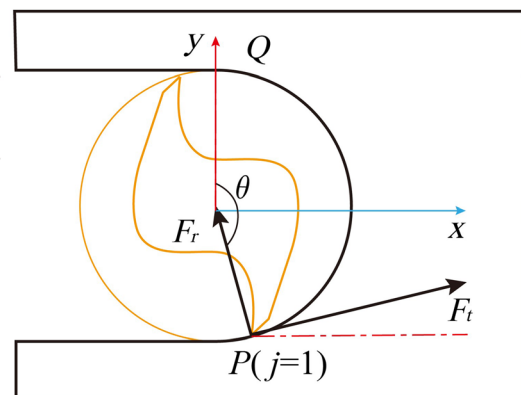
By integrating the  $dF_x$ ,  $dF_y$ , and  $dF_a$  along the cutting edges, the resultant cutting forces in the  $x$ ,  $y$ , and  $z$  directions can be obtained as follows:

$$\begin{cases} F_x(\theta) = \int_{\theta_l}^{\theta_u} (-K_{tc}h(\theta) + K_{te})\cos(\theta) - (K_{rc}h(\theta) + K_{re})\sin(\theta) \frac{R}{\tan\beta} d\theta \\ F_y(\theta) = \int_{\theta_l}^{\theta_u} ((K_{tc}h(\theta) + K_{te})\sin(\theta) - (K_{rc}h(\theta) + K_{re})\cos(\theta)) \frac{R}{\tan\beta} d\theta \\ F_a(\theta) = \int_{\theta_l}^{\theta_u} (K_{ae} + K_{ac}h(\theta, z)) \frac{R}{\tan\beta} d\theta \end{cases} \quad (5)$$

where  $\theta_l$  and  $\theta_u$  are the lower and upper integration limit angles. The relationship between  $\theta_l$  and  $\theta_u$  can be expressed by:

$$\theta_u = \theta_l + \frac{a_p \tan\beta}{R} \quad (6)$$

where  $a_p$  and  $\theta_l$  represent the cutting depth and rotation angle on the end face of cutting tool, respectively.  $R$  represents actual cutting radius.



Due to helix angle effect, cutting area is divided into three zones named as entry, intermediate, and exit zones, as shown in Fig. 3. Only in the intermediate zone is the cutting edge fully engaged into cutting. Integration limit in different cutting areas is shown in Table 1, where  $\theta_s$  and  $\theta_e$  represent start and exit angles, which will be discussed in the following sections.

### 2.2 Tool runout effect

The ideal situation is that the geometry center of cutting tool should coincide with the spindle rotation center. However, due to manufacture tolerance and installation errors, the tool geometry center always deviates from the rotation center, which makes the effective radius of cutting tools different from nominal dimension, and tool runout phenomenon occurs [29]. In conventional milling, feed per tooth usually varies from dozens of microns to several millimeters. The tool runout is usually less than 1 $\mu$ m. Thus, the effect of tool runout is negligible in conventional milling process. However, in micro-milling process, the feed per tooth is usually just several microns or less, which is comparable to tool runout and will significantly influence the cutting force in micro end milling. Besides, due to lower strength and stiffness of micro-tools, runout will also cause much more vibration.

The cutting tool moves in a curve of uniparted hyperboloid due to tool runout and tilt. Since the cutting tool has two degrees of freedom including rotation about the  $z$  axis and transition along the  $z$  axis, four parameters need to be determined in order to describe the cutting tool spatial position and orientation, as shown in Fig. 4. Space angle of cutting tool and rotation axis is defined by  $\gamma$ .  $\lambda$  is measured when the cutting tool is paralleled with the  $yz$  plane. Axial offset and runout phase angle are defined by  $r$  and  $\tau$  in end face of cutting tool. Cutting depth in micro end milling usually varies from several to dozens of micrometers, which is negligible compared to tool length. Hence, the tool runout  $r$  can be considered as a constant during milling process.

Cutting tool radii ( $NP$  and  $NQ$ ) are the same in ideal situation. However, due to tool runout effects, actual cutting radii  $MP$  and  $MQ$  are different, which are hard to be measured directly. The difference between  $MP$  and  $MQ$  can be obtained directly by displacement sensor.  $\phi$  and  $\tau$  can be calculated from the result of displacement sensor, where  $\phi$  represents the phase difference of two cutting radii. According to Fig.

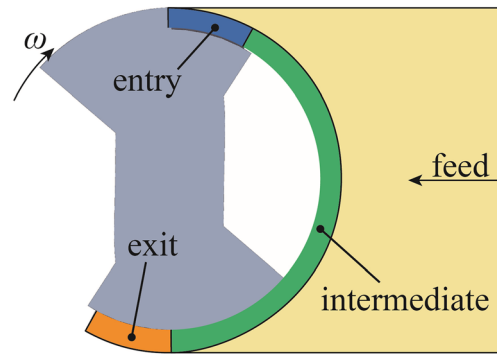


Fig. 3 Entry, intermediate, and exit zone

4, Eqs. (7) and (8) can be obtained according to cosine formula:

$$\cos(\varphi) = \frac{MQ^2 + MP^2 - PQ^2}{2 \cdot MQ \cdot MP} \tag{7}$$

$$\cos(\tau) = \frac{MN^2 + MP^2 - PN^2}{2 \cdot MN \cdot MP} \tag{8}$$

where  $PN$  is ideal cutting tool's radius  $R$ .

In order to obtain runout phase angle  $\tau$ , two laser displacement sensors are fixed along the  $z$  axis at the height of rotational axis as shown in Fig. 5. Cutting tool rotates about point  $M$ . Laser sensor 1 returns two different minimum values when  $MP$  and  $MQ$  lie collinear with  $MB$ . Laser sensor 2 returns a maximum value when  $MN$  lies collinear with  $MB$ . By comparing the results of laser sensor 1 and 2,  $\tau$  and  $\phi$  can be calculated. The relationship between  $MQ$  and  $MP$  is given by:

$$\Delta = MP - MQ \tag{9}$$

where  $\Delta$  is peak difference of laser sensor 1 and it can be obtained in experiment.

Substituting Eq. (9) into Eq. (7),  $MP$  can be calculated by:

$$MP = \frac{\sigma_1 - \Delta + \Delta \cos(\varphi)}{2(\cos(\varphi) - 1)} \tag{10}$$

where  $\sigma_1$  can be expressed as:

$$\sigma_1 = \sqrt{(\cos(\varphi) - 1)(\Delta^2 - 8R^2 + \Delta^2 \cos(\varphi))} \tag{11}$$

Substituting Eq. (11) into Eq. (8), tool runout  $MN$  can be calculated as:

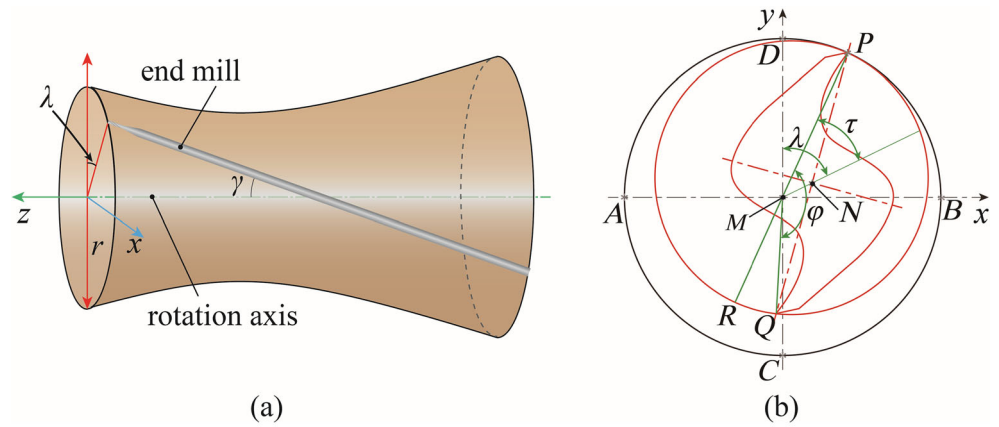
$$MN = \cos(\tau)MP - \sqrt{\cos(\tau)^2 MP^2 + R^2 - MP^2} \tag{12}$$

From Eq. (11), it is noted that actual cutting radius varies along the  $z$  axis due to tool runout and helix angle. As shown in Fig. 6, point  $N$  is geometry center of cutting tool.  $R_1$  and  $R_s$  represent the longer and shorter actual cutting radii in section  $\triangle MPQ$ .  $R_1'$  and  $R_s'$  represent the longer and shorter actual cutting radii in section  $\triangle MP'Q'$ .

Table 1 Integration limits in different cutting areas

Cutting area	$\theta_l$	$\theta_u$
Entry	$\theta_s$	$\theta$
Intermediate	$\theta - \frac{a_r \tan \beta}{R}$	$\theta$
Exit	$\theta$	$\theta_e$

**Fig. 4** Model of tool runoff: **a** axis offset and tilt, **b** tool runoff in end face



Ideal cutting radius  $PN$  rotates to line  $P'N$  in section  $M'P'Q$ . Rotation angle about point  $N$  can be expressed as follows:

$$\angle P'NP = \frac{z \tan \beta}{R} \tag{13}$$

where  $z$  is the distance from current section to end face along  $z$  axis.

By solving above equations,  $R_1'$  and  $R_s'$  can be given as follows:

$$\begin{cases} R_1' = \sqrt{-2 \cos(\angle MNP - \angle P'NP) r_0 R + R^2 + r_0^2} \\ R_s' = \sqrt{-2 \cos(\pi - \angle MNP + \angle P'NP) r_0 R + R^2 + r_0^2} \end{cases} \tag{14}$$

**Fig. 5** Method of tool runoff measurement

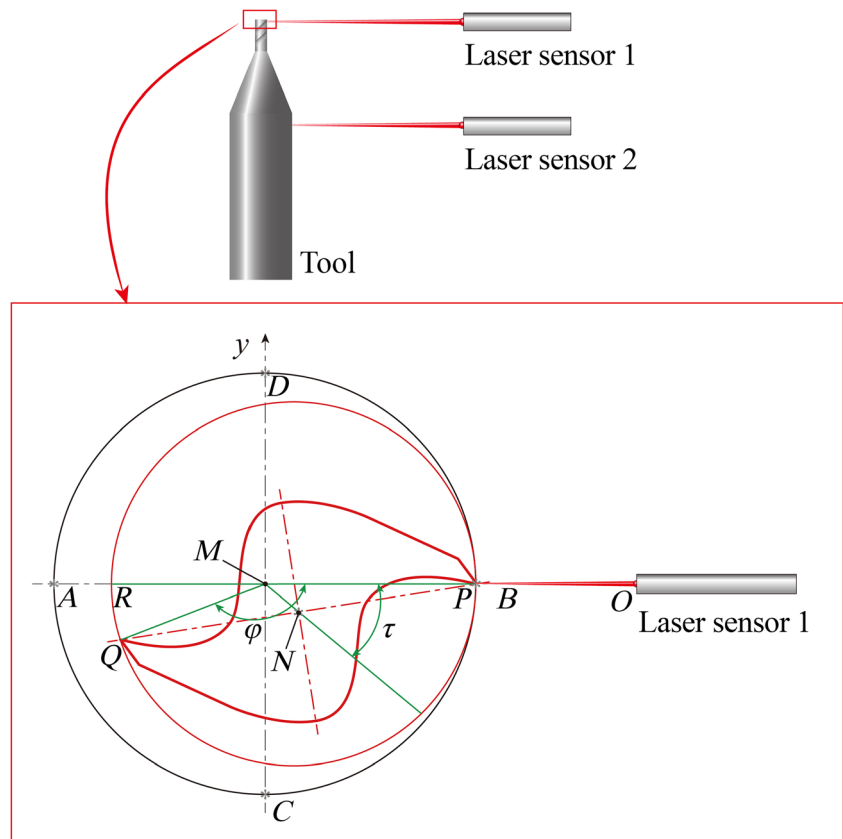
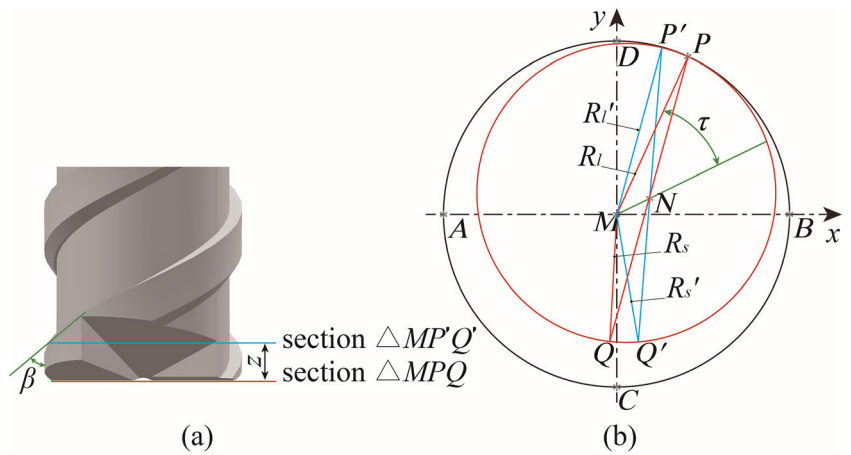




**Fig. 6** Actual cutting radius of different  $z$  position, **a** section position, **b** cutting radius on different sections



**2.3 Algorithm for calculating instantaneous uncut chip thickness**

The cutting force is determined by instantaneous uncut chip thickness. Thus, a precise algorithm for instantaneous uncut chip thickness is necessary for cutting force calculation. Conventional instantaneous uncut chip thickness can be approximately expressed as:

$$h(\theta) = f_z \sin(\theta) \tag{15}$$

where  $f_z$  is feed per tooth.

Equation (15) is generally used to calculate the resultant cutting force in macro end milling for its conciseness. However, the tool runout and tool deflection are comparable to feed per tooth in micro end milling. These effects should be considered in instantaneous uncut chip thickness calculation.

Figure 6 demonstrates the cutting edge trajectory with consideration of tool runout. The position of cutting tool’s geometric center (green line) can be calculated by:

$$\begin{cases} x = ft + r_0 \sin(\omega t + \tau) \\ y = r_0 \cos(\omega t + \tau) \end{cases} \tag{16}$$

where  $r_0$  and  $\omega$  denote the tool runout and angular velocity of cutting tool, respectively.  $t$  is the cutting time. The trajectory of cutting edges (blue and red lines) can be calculated by Eqs. (18) and (19).

$$\begin{cases} x_s = ft + R_s \sin(\omega t + \varphi) \\ y_s = R_s \cos(\omega t + \varphi) \end{cases} \tag{17}$$

$$\begin{cases} x_l = ft + R_l \sin(\omega t) \\ y_l = R_l \cos(\omega t) \end{cases} \tag{18}$$

where  $x_s$  and  $y_s$  represent coordinate of shorter cutting edge and  $x_l$  and  $y_l$  represent coordinate of longer cutting edge.

As shown in Fig. 7, cutting areas of first and second cutting edges are shown as blue and orange shadows, respectively.

Under ideal condition, the blue line  $ABCD$  left by cutting edge 1 should be removed by cutting edge 2. However, due to tool runout, the actual cutting edge’s radius is different, and the blue line is removed from  $B$  to  $C$ ; line segments  $AB$  and  $CD$  are formed and removed only by cutting edge 2, making two cutting edges’ instantaneous uncut chip thickness different.

One single turn is chosen to model the instantaneous uncut chip thickness, because the cutting process is endless repetitions. Blue line  $ABCD$  is assumed to be the start surface. At time  $t_k$ , the cutting edge 1 is located at point  $P$  as shown in Fig. 9.  $Q$  represents the intersection point of  $R_s$  and start surface.  $PQ$  is considered to be the instantaneous uncut chip thickness. The coordinate of rotation center  $O_{tk}$  is calculated as:

$$\begin{cases} x_o = ft_s \\ y_o = 0 \end{cases} \tag{19}$$

With coordinate of  $O_{tk}$  and slope of line  $PO_{tk}$ ,  $PO_{tk}$  can be given as:

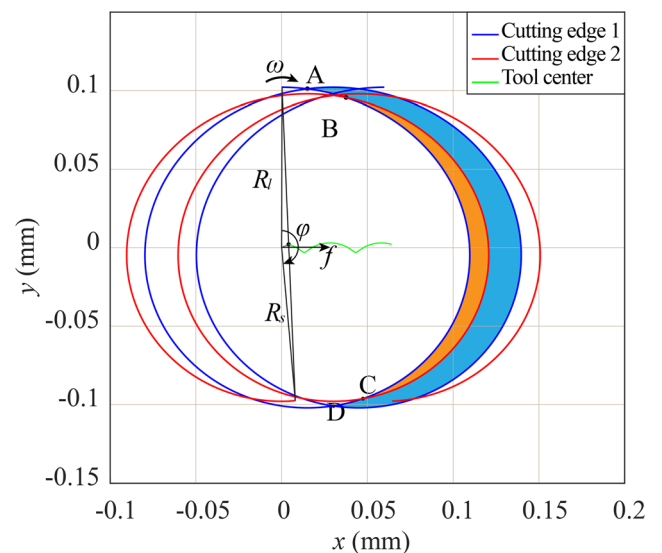


**Fig. 7** Cutting edge trajectory

$$y = (x - ft_s) / \tan(\omega t_s + \varphi) \tag{20}$$

Substituting Eq. (18) into Eq. (20), a function about  $t$  can be calculated by:

$$f(t) - R_l \cos(\omega t) - (ft + R_l \sin(\omega t) - ft_s) / \tan(\omega t_s + \varphi) = 0 \tag{21}$$

Newton’s iteration method is utilized to solve the equation because  $f(t)$  is a nonlinear equation of  $t$ . The basic form of Newton’s iteration method is given as:

$$t_{k+1} = t_k - \frac{f(t_k)}{f'(t_k)} \tag{22}$$

where  $t_k$  is initial solution and  $f'(t_k)$  is the derivative of  $f(t)$  at point  $t_k$ , which can be expressed as:

$$f'(t) = -R_l \omega \sin(\omega t) - (f + R_l \omega \cos(\omega t) f t_s) / \tan(\omega t_s + \varphi) \tag{23}$$

A proper initial value of  $t_k$  is important for the Newton’s iteration method. Considering the phase difference of two cutting edges,  $t_0$  is chosen as the initial value of  $t$  and given by:

$$t_0 = t_s - \frac{2\pi}{\omega N_0} \tag{24}$$

For any precision  $\epsilon$ , the solution of  $t_1$  can be solved according to Fig. 8.

When  $R_l$  is engaged in cutting, as drawn by  $RO_{II}$  in Fig. 9, the instant uncut chip thickness consists of two parts including curve  $AB$  and curve  $BF$ . At time  $t_1$ ,  $R_l$  is placed coincide with line  $RO_{II}$ , which can be expressed as:

$$y = (x - ft_1) / \tan(\omega t_1) \tag{25}$$

Substitute Eqs. (17) and (18) into Eq. (25), respectively, Eq. (27) can be obtained:

$$\begin{cases} f(t_{s1}) = R_s \cos(\omega t_{s1}) - (ft_{s1} + R_s \sin(\omega t_{s1}) - ft_1) / \tan(\omega t_1) = 0 \\ f(t_{s2}) = R_s \cos(\omega t_{s2} + \varphi) - (ft_{s2} + R_s \sin(\omega t_{s2} + \varphi) - ft_1) / \tan(\omega t_1) = 0 \end{cases} \tag{26}$$

Finally, instantaneous uncut chip thickness can be calculated with  $t_{s1}$  in section  $AB$  and  $t_{s2}$  in section  $BF$ .

A series of  $t_1$  can be calculated for a series of corresponding  $t_s$  along curve  $ABCD$ . The instantaneous uncut chip thickness of  $R_s$  and  $R_l$  can be expressed as:

$$h_{ts} = (x_{ts} - x_{tl}) / \tan(\omega t_s + \varphi) \tag{27}$$

$$h_{tl} = \min\{(x_{tl} - x_{ts1}) / \tan(\omega t_1), (x_{tl} - x_{ts2}) / \tan(\omega t_1)\} \tag{28}$$

A positive value of  $h_{ts}$  means cutting is in process, while a negative  $h_{ts}$  means not. The critical value between positive and negative value means start angle or end angle.

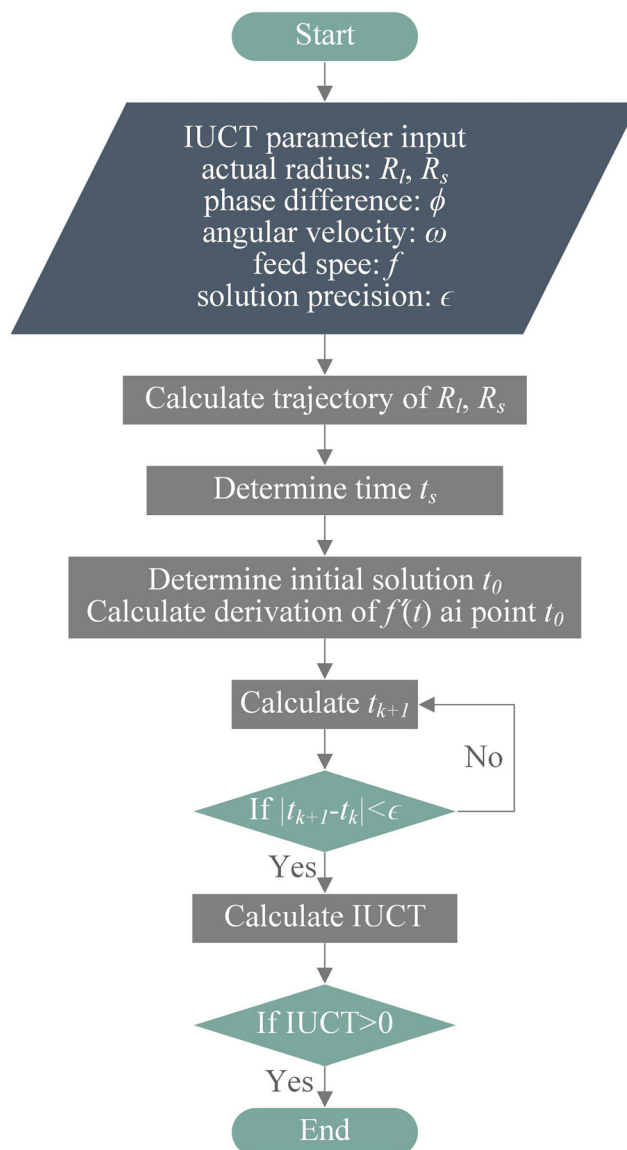


Fig. 8 Flowchart for calculating instantaneous uncut chip thickness

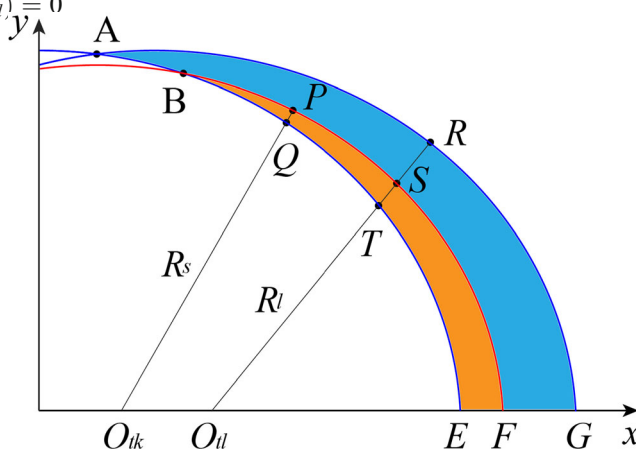


Fig. 9 Model of instantaneous uncut chip thickness calculation

Instantaneous uncut chip thickness of each element can be calculated in the same process.

### 2.4 Identification of cutting force coefficients

Cutting force coefficients will be estimated based on the cutting force model in this section. It should be noted that the cutting depth is constant during a slot milling process. The cutting force component is proportional to instantaneous uncut chip thickness. Thus, the resultant cutting force during the whole milling process is proportional to removal material volumes in a single turn of cutting tool. Without considering tool runout, removal material volumes are relative only to feed per tooth in case the cutting tool’s radius is determined. The proportion coefficients are relative only to the cutting force coefficients  $K_{tc}$ ,  $K_{rc}$ , and  $K_{ac}$ . Thus, the helix angle can be no longer considered in the resultant force. To reduce the complexity of the formula, instantaneous uncut chip thickness can be approximately written as Eq. (15) because the removal material volume should be cared rather than the instantaneous value of uncut chip thickness.

Substituting Eq. (1) into Eq. (2), the component force  $dF_{x_{ij}}$  and  $dF_{y_{ij}}$  can be calculated as:

$$\begin{cases} dF_x = -(K_{tc}h(\theta) + K_{te})\cos(\theta) - (K_{rc}h(\theta) + K_{re})\sin(\theta)dz \\ dF_y = ((K_{tc}h(\theta) + K_{te})\sin(\theta) - (K_{rc}h(\theta) + K_{re})\cos(\theta))dz \end{cases} \quad (29)$$

Taking integration of Eq. (29) from  $z=0$  to  $z=a_p$ , instantaneous cutting force of a single cutting edge can be calculated as follows:

$$\begin{cases} dF_x = -(K_{tc}h(\theta) + K_{te})\cos(\theta) - (K_{rc}h(\theta) + K_{re})\sin(\theta)a_p \\ dF_y = ((K_{tc}h(\theta) + K_{te})\sin(\theta) - (K_{rc}h(\theta) + K_{re})\cos(\theta))a_p \end{cases} \quad (30)$$

where  $a_p$  is the cutting depth.

Taking integration of instantaneous cutting force on  $\theta$ , total force of a single cutting edge during one turn can be calculated by:

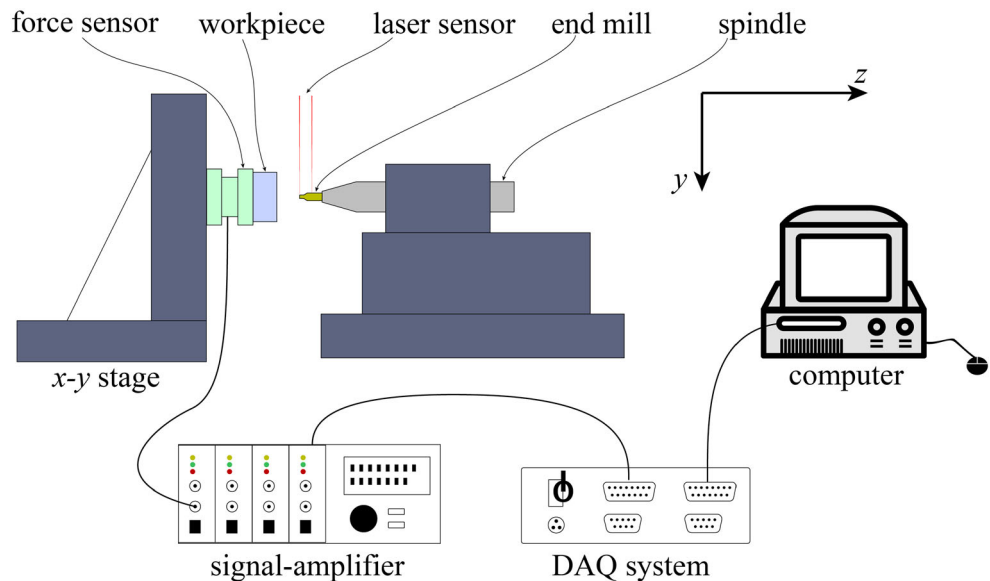
$$\begin{cases} F_{x_{sum}} = \int_0^\pi (-(K_{tc}h(\theta) + K_{te})\cos(\theta) - (K_{rc}h(\theta) + K_{re})\sin(\theta))a_p d\theta \\ F_{y_{sum}} = \int_0^\pi ((K_{tc}h(\theta) + K_{te})\sin(\theta) - (K_{rc}h(\theta) + K_{re})\cos(\theta))a_p d\theta \\ F_{z_{sum}} = \int_0^\pi (K_{ac}h(\theta) + K_{ae})a_p d\theta \end{cases} \quad (31)$$

Integration limits of Eq. (31) vary from 0 to  $\pi$ , which are ideal entry and exit angles. Two cutting edges’ cutting conditions are all the same without considering tool runout effect. By simplifying Eq. (31), the following equation can be obtained:

$$\begin{cases} F_x = -\frac{K_{rc}a_p\pi}{2}f_z - 2a_pK_{re} \\ F_y = \frac{K_{tc}a_p\pi}{2}f_z + 2a_pK_{te} \\ F_z = 2K_{ac}a_p f_z + a_p\pi K_{ae} \end{cases} \quad (32)$$

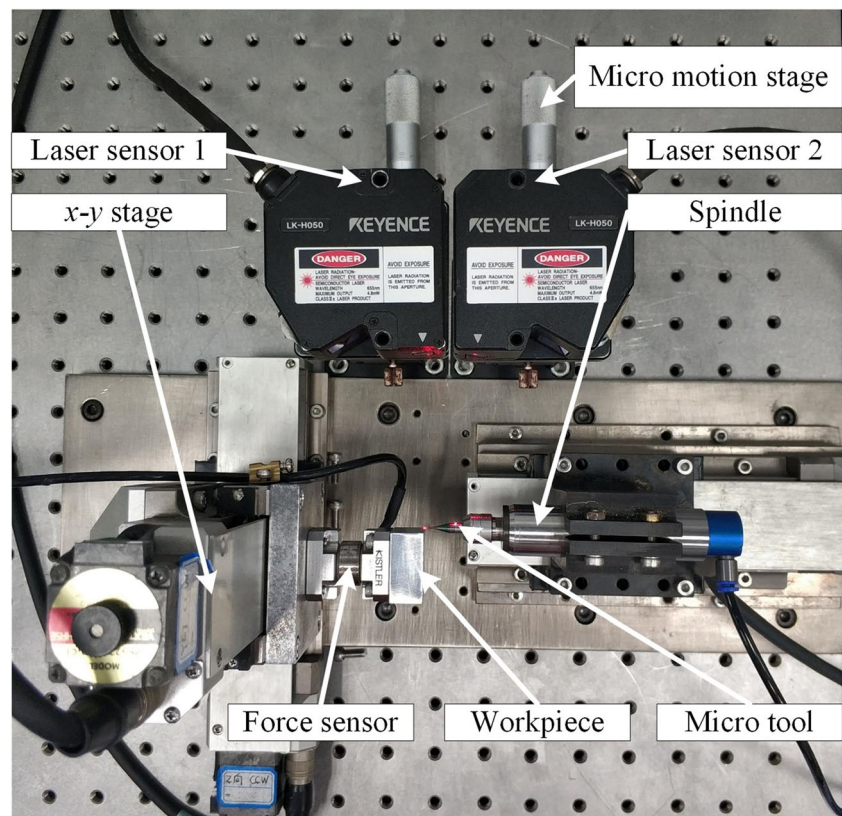
Equation (32) indicates that resultant force components are a linear function of  $f_z$ , and the slopes are relative only to cutting force coefficients, and intercepts are relative only to cutting edge coefficients. The cutting force coefficients can be estimated with a linear fit of cutting force and feed per tooth.

Fig. 10 Schematic diagram of experimental setup





**Fig. 11** Actual setup of experiment



### 3 Experimental setup

The validation of cutting force model is conducted by a series of micro slot end milling process. The details of experiment setup will be explained in this section. It should be pointed out in advance that due to size effect, the experiment is carried out in a small feed speed range to obtain cutting coefficients.

In order to verify the precision of cutting force model proposed above, a self-build machining system is used to conduct experiments. Two-edged solid carbide miniature end mills with radius of 0.2 mm and 0.4 mm (Karnasch Art. 3062020040010) are employed to perform end milling on copper alloy (T2Y). Helix angle of cutting tool is  $30^\circ$ . The workpiece is attached on a 3-component force sensor (Kistler 9317B), which has a sensitivity of  $-26\text{pC/N}$  in the  $x$ - $y$  direction and  $-11\text{pC/N}$  in the  $z$  direction. Natural frequency of the force sensor is 5 kHz, and linearity error is less than 0.5% of full scale. Force sensor is mounted on a  $x$ - $y$  linear stage with a high linearity of  $3\mu\text{m}$  and a resolution of  $1\mu\text{m}$ . In order to achieve a required cutting speed, an electric spindle (Nakanish BM 320) is used to perform milling process which has a max speed of 80,000 rpm and spindle runout less than  $1\mu\text{m}$ . Schematic diagram of experiment is shown in Fig. 10.

Force measurement system is made up of an 8-channel charge amplifier (Kistler type 5080A) and a DAQ system (Kistler type 5697A). The signal drift of charge amplifier

under DC measuring mode is less than  $\pm 0.03\text{mV/s}$ . Thus, force acquisition is conducted separately in every feed procedure to avoid signal drift. DAQ system has a maximum sampling rate of 333kS/s with resolution of 16 bit for each channel. Two laser sensors with a repeatability of  $0.025\mu\text{m}$  (Keyence LK-H050) are placed in a plane parallel with  $z$  axis to measure tool runout before cutting as shown in Fig. 11. In order to make sure laser sensors focus on the rotation axis, two  $y$  axis micro motion stages are used to mount laser sensors. Two laser sensors focus on the tool tip and tool shank, respectively, to obtain runout phase angle. Blunt radius of end mills is measured by Edge Master G4 Vc6 of Alicona. Cutting parameters are shown in Table 2.

## 4 Results and discussions

### 4.1 Cutting force coefficients

Results of blunt radius measurement are shown in Fig. 12. Two different cutting radius end mills have similar blunt radii

**Table 2** Cutting parameters of experiment

Cutting depth	Spindle speed	Tool radius	Sample frequency
$50\mu\text{m}$	15,000rpm	0.2mm, 0.4mm	80,000Hz

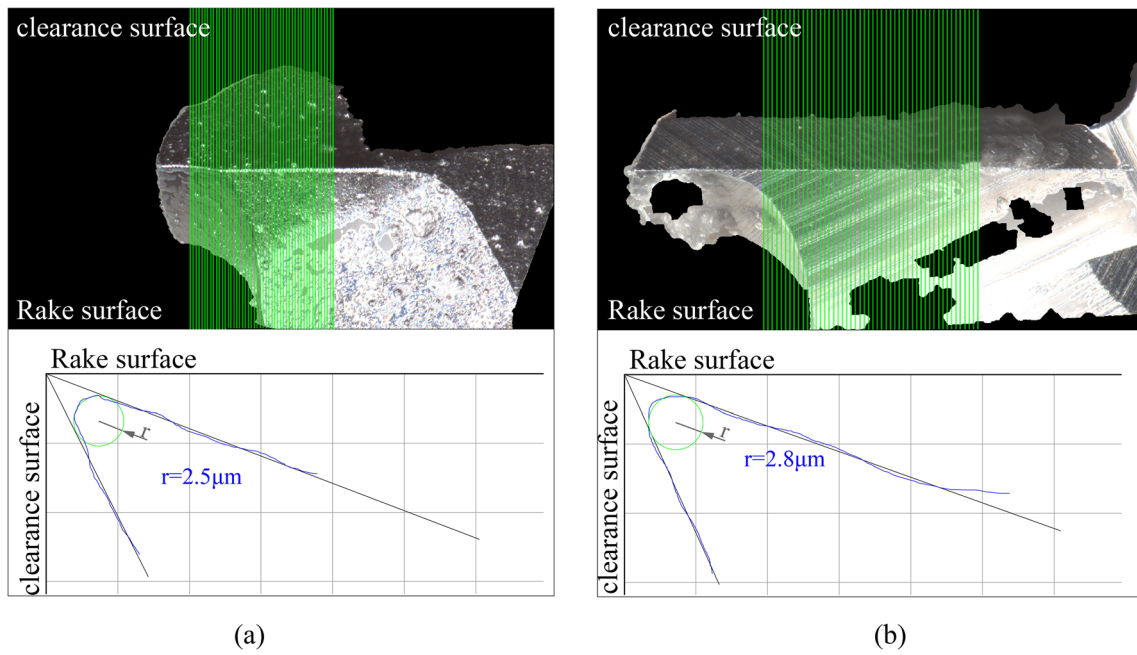


Fig. 12 Measure result of blunt radius: **a** blunt radius of end mill  $R=0.2\text{mm}$ , **b** blunt radius of end mill  $R=0.4\text{mm}$

of  $2.5\mu\text{m}$  and  $2.8\mu\text{m}$ . The average cutting forces in different cutting parameters are shown in Fig. 13. Three linear models are used to analyze the influence of feed per tooth using Eq. (32). Three models' coefficients are 0.9377, 0.9779, and 0.9792, respectively, which means force data has a good linear correlation. Cutting coefficients vary with tool's diameter as

shown in Table 3 even if they have similar blunt radii. A tool with a smaller blunt radius has larger cutting force coefficients. It can be explained with the fact that the contact length is larger at larger radius, which creates more friction. Besides, cutting coefficients may also be affected by manufacturing technique of cutting tools.

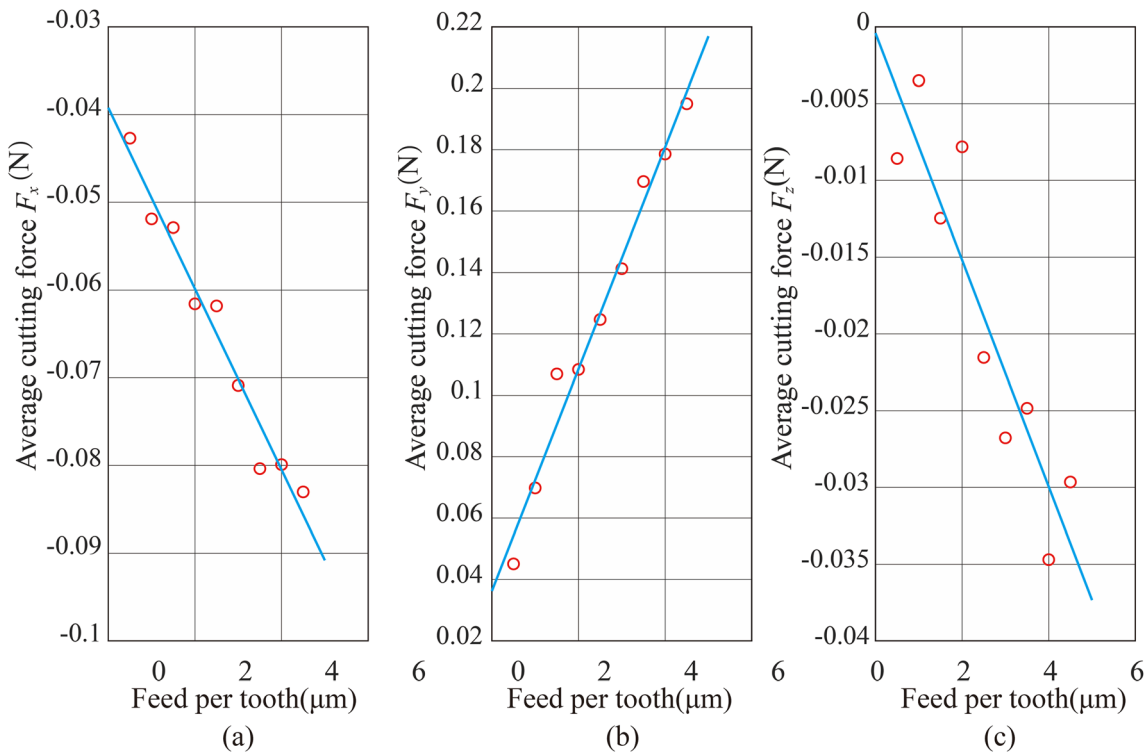


Fig. 13 Average cutting force of 0.2-mm radius end mill at different feed speeds: **a** average cutting force in  $x$  direction, **b** average cutting force in  $y$  direction, **c** average cutting force in  $z$  direction

**Table 3** Cutting coefficients of different end mills

Cutting coefficient	Ktc	Krc	Kac	Kte	Kre	Kae
	KN/mm <sup>2</sup>	KN/mm <sup>2</sup>	KN/mm <sup>2</sup>	N/m	N/m	N/m
0.2-mm radius end mill	1446	413	232	1.14	1.23	-0.008
0.4-mm radius end mill	2088	1083	268	2.43	3.49	0.34

### 4.2 Tool runout measurement

Figure 14 shows the result of tool runout measurement. Blue line has two peaks of different values during one revolution because of tool runout effect, corresponding to  $R_1$  and  $R_s$  in Fig. 6. Besides, phase difference of two peaks in the same line is not perfect 180°.  $\tau$  is indicated by a difference of two different line peaks in Fig. 4. The difference of actual cutting radii  $MP$  and  $MQ$  can be measured directly in the diagram. Real cutting radii  $R_1$  and  $R_s$  are calculated to be 0.4003 mm and 0.3997 mm using Eqs.(7)–(14).

The influence of  $\tau$  and  $r_0$  on actual cutting radius  $R_1$  is shown in Fig. 15. Tool runout  $r_0$  limits range of  $R_1$  and phase angle  $\tau$  affects the value of cutting radius. When  $\tau$  is about  $\pi/2$ , the tool runout has negligible effect on actual cutting radius. When phase angle equals to 0 or  $\pi$ , the change of actual cutting radius reaches to maximum value, and the difference between two cutting edge equals to twice of  $r_0$ , which will increase the unevenness of tool wear. It is hard to fully eliminate the  $r_0$  in actual installation, but it can be reduced by adjusting phase angle  $\tau$ . Besides, a cutting tool with more cutting edges can reduce the differences among cutting edges and has a better performance in cutting process.

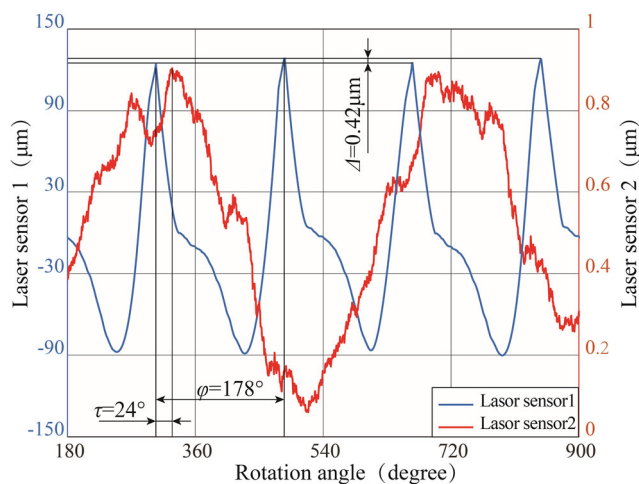


**Fig. 14** Experiment data of tool runout measurement ( $r=0.4\text{mm}$ )

The influence of  $\tau$  and  $r_0$  on instantaneous uncut chip thickness in different situations is shown in Fig. 16.  $h(\theta)$  represents instant uncut chip thickness. When cutting tool’s geometry center is placed perfectly at the rotation center, two cutting edges’  $h(\theta)$  is completely identical as shown in Fig. 16a. Figure 16b and c show the influence of tool runout and runout phase angle. The difference between two cutting edges rises with increasing of  $r_0$  and decreasing of  $\tau$ , and  $\tau$  has a more significant effect on  $h(\theta)$ . It can be inferred that  $h(\theta)$  will reduce to zero with  $r_0$  increasing; then single-edge cutting occurs. Besides, the cutting edge which removes more material will have more severe wear.

Tool runout has a significant impact on entrance angle and exit angle of  $R_s$  but has little effect on  $R_1$ . As shown in Fig. 17, where  $\theta_{1s}$ ,  $\theta_{1e}$ ,  $\theta_{ss}$ , and  $\theta_{se}$  represent entrance angle of  $R_1$ , exit angle of  $R_1$ , entrance angle of  $R_s$ , and exit angle of  $R_s$ . The former surface is formed by  $R_1$  itself when  $R_1$  rotates into workpiece, which can be illustrated by point A in Fig. 9. Thus, the difference between two cutting radii has little effect on  $\theta_{1s}$  and  $\theta_{1e}$ , which is caused by tool runout. Entrance and exit angles of  $R_1$  are related only to feed speed, and they should be 180° and 360° when feed speed equals to zero. However, when  $R_s$  rotates into workpiece, the former surface is formed by  $R_1$ , which can be illustrated by point B in Fig. 9. Difference of  $R_s$

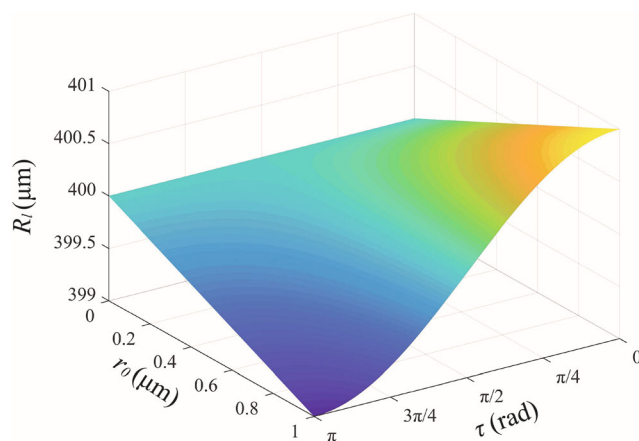


**Fig. 15** Influence of  $\tau$  and  $r_0$  on  $R_1$

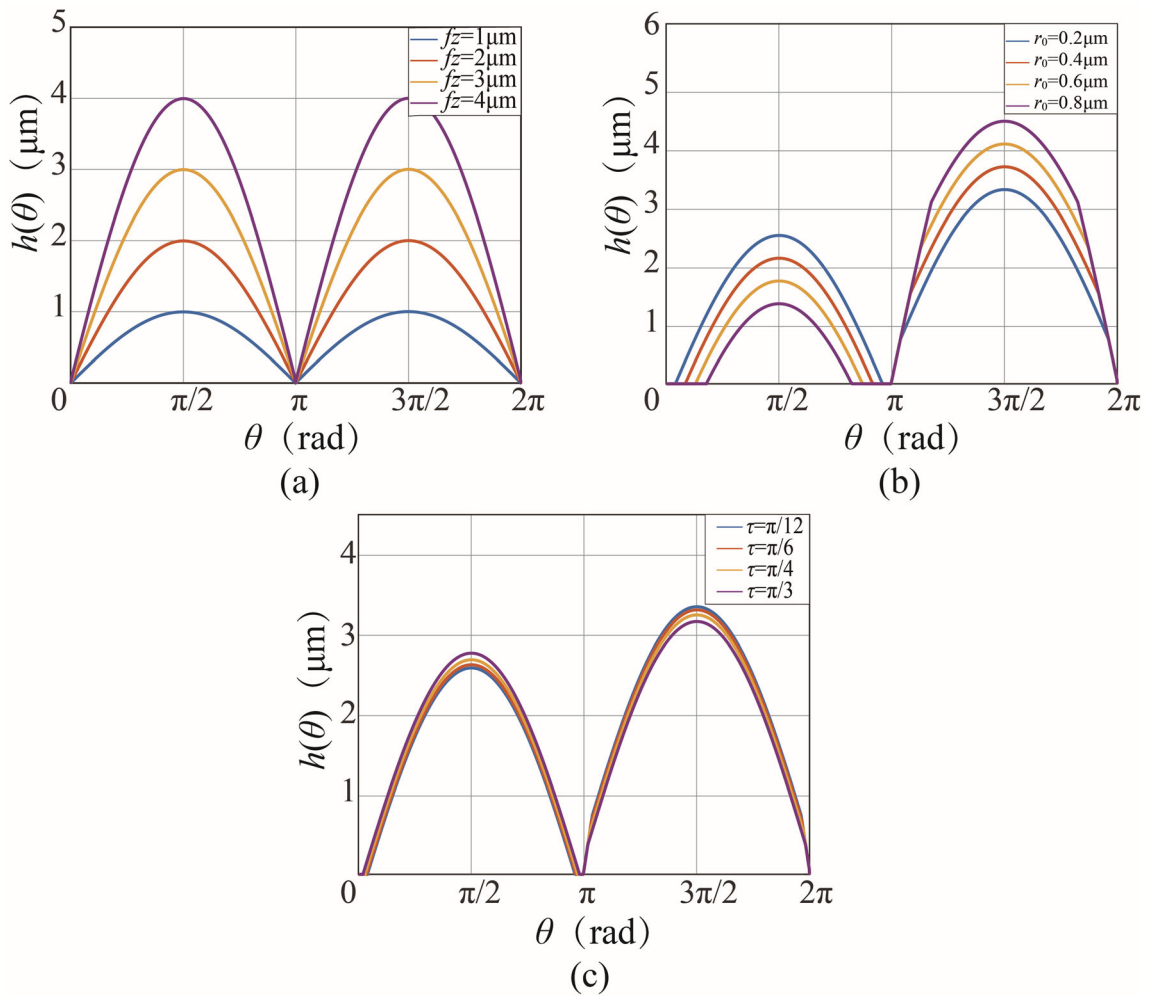


**Fig. 16**  $h(\theta)$  in different situations: **a**  $h(\theta)$  of different feed per tooth  $f_z$  ( $R=0.2\text{mm}$ ), **b**  $h(\theta)$  of different runout  $r_0$  ( $R=0.2\text{mm}, f_z=3\text{mm}$ ), **c**  $h(\theta)$  of different runout phase angle  $\tau$  ( $R=0.2\text{mm}, f_z=3\text{mm}, r_0=0.2\mu\text{m}$ )

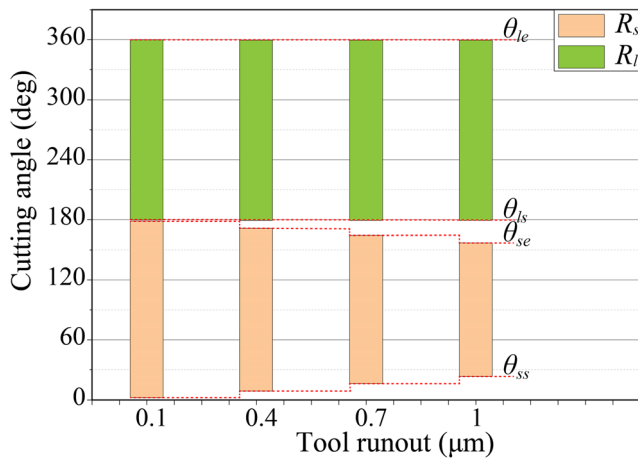


**Fig. 17** Cutting angle of  $R_s$  and  $R_l$  at different tool runouts

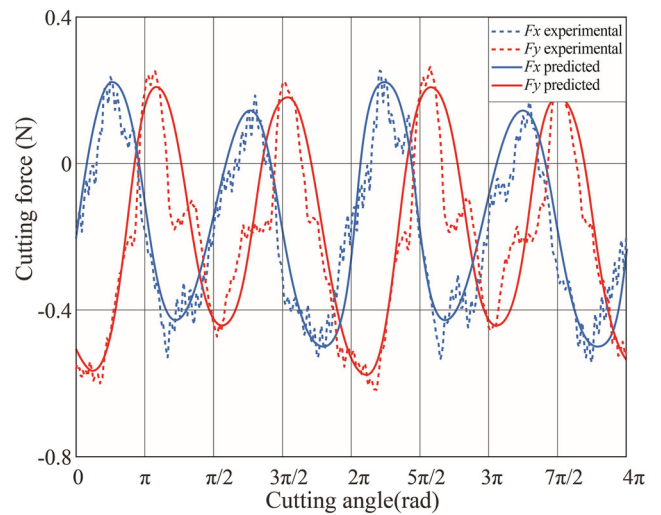


**Fig. 18** Comparison of predicted and experiment cutting forces ( $f_z=2\text{mm}$ )



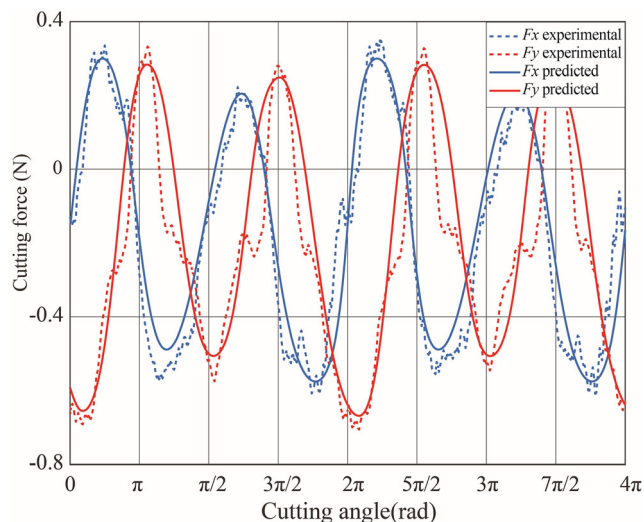


Fig. 19 Comparison of predicted and experiment cutting forces ( $f_z=3 \mu\text{m}$ )

and  $R_1$  will rise with tool runout increasing, causing a larger entrance angle and smaller exit angle.

### 4.3 Cutting force model validation

Figures 18 and 19 show the comparisons of predicted cutting forces and experimental results in different feed speeds.  $F_x$  and  $F_y$  are depicted with blue and red lines, respectively, and experimental force and predicted force are plotted by dotted lines and solid lines, respectively. There are two different peaks in one revolution because of tool runout effect; the longer cutting radius tends to have more uncut chip thickness and bear larger cutting force. The difference between the maximum value of predicted and experimental cutting forces in

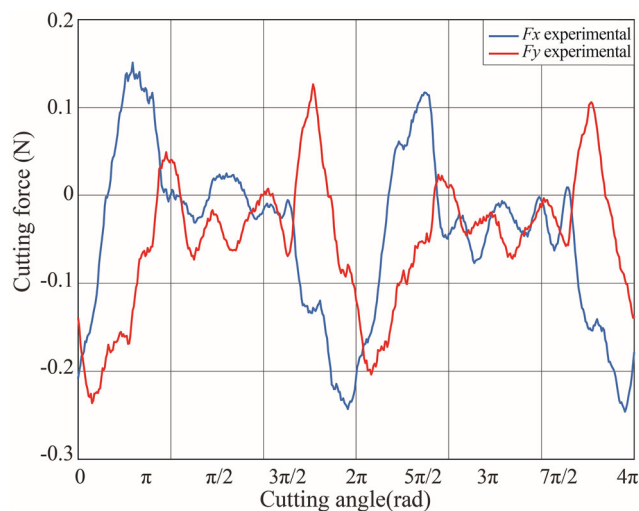


Fig. 20 Cutting force in the  $x$  and  $y$  directions ( $f_z=0.5 \mu\text{m}$ )

different feed speed is less than 8%, which is in good agreement with the research of Zhang et al. [7].

Cutting force in  $z$  direction is not presented because it is negligible compared to  $x$  and  $y$  directions. It has been shown by Mittal et al. that axial cutting force has no significant effect to regenerative chatter [30].

Fig. 20 shows experimental cutting forces in  $x$  and  $y$  directions when  $f_z$  is  $0.5 \mu\text{m}$ . Theoretical cutting force should have only one peak in one revolution because the difference of  $R_1$  and  $R_s$  is larger than  $0.5 \mu\text{m}$ . However, experimental result has a smaller peak because longer cutting edge will have more elastic deformation than the other, which makes actual difference between  $R_1$  and  $R_s$  slightly smaller than  $0.6 \mu\text{m}$ . Besides,  $h(\theta)$  is not only affected by the tool’s trochoidal trajectory, deflection, and tool runout, but also affected by the shape of previous formed surface including the chip thickness accumulation [31]. Hence, a smaller peak appears in Fig. 20.

Fig. 21 shows cutting forces in  $x$  and  $y$  directions of different  $\tau$  when  $f_z$  is  $2 \mu\text{m}$  and tool runout equals to  $0.3 \mu\text{m}$ . With increasing of  $\tau$ , the difference of two peaks during one revolution decreases, and two cutting edges have similar peak values until  $\tau$  equals to  $\pi/2$ . It indicates that the effect of tool runout can be reduced by adjusting  $\tau$ .

## 5 Conclusion

In the paper, an accurate cutting force model in micro end milling has been developed based on a novel algorithm of instant uncut chip thickness. This model is fully based on experimental data and takes tool runout effect and minimum chip thickness into consideration. Based on the investigations conducted, the following conclusions can be obtained:

- A new method is proposed to measure tool runout in micro end milling using laser displacement sensor. To avoid the effect of tool tilt, tool runout is measured at the end face instead of tool shank.
- The tool is assumed to exist a parallel offset from rotation axis for calculating instant uncut chip thickness. The offset distance and phase angle are used to redefine cutting radii, which are used to calculate trajectory of cutting edge. Offset distance affects the actual instant uncut chip thickness, while runout phase angle determines the influence of offset distance. By adjusting runout phase angle, the influence of tool runout can be diminished.
- Entry angle and exit angle are calculated according to instant uncut chip thickness. Tool runout affects only one cutting edge and has few influences on the other.



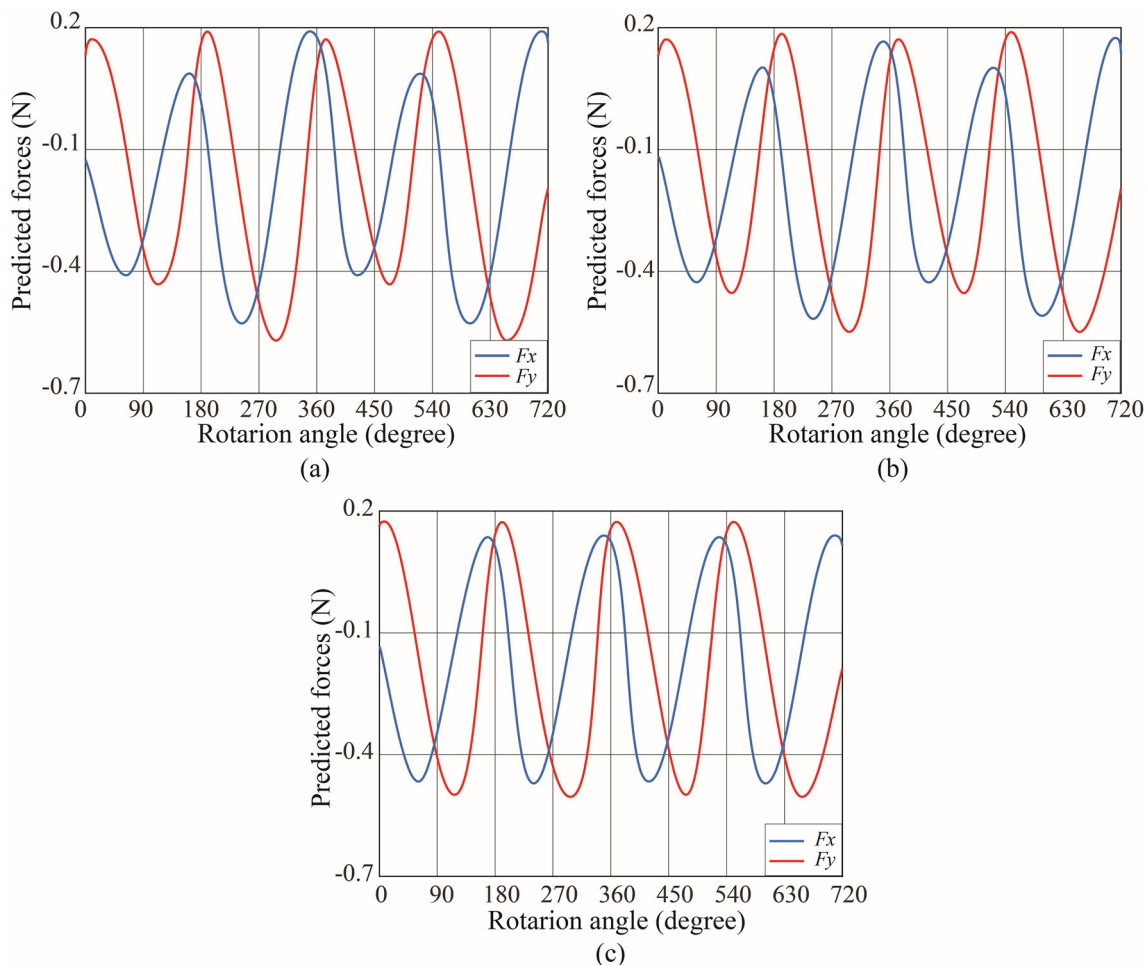


**Fig. 21** Predicted cutting forces with different  $\tau$  when  $f_z=2\mu\text{m}$ ,  $r_0=0.3\mu\text{m}$ . **a**  $\tau=0$ . **b**  $\tau=\pi/4$ . **c**  $\tau=\pi/2$

- An experiment-based method is used to determine cutting coefficients. This method performs well in micro end milling though it was used in macro end milling. Maximum deviation between predictive and experimental cutting forces is less than 8%.
- Cutting coefficients vary with blunt radius of tools, and larger blunt radius tends to have larger cutting coefficient. Even the same type of tools may have different cutting coefficients due to machining technology.

**Author contribution** Weijie Wang: Conceptualization, methodology, investigation, and writing. Weiwei Zhang: Resources and supervision. Dingchuan Huang: Data curation and original draft. Wei Wang: Validation and investigation.

**Funding** The authors gratefully acknowledge the supports of the Laboratory of Precision Manufacturing Technology (CAEP. NO. ZM18007).

**Data availability** All data generated or analyzed during this study are included in this article.

## Declarations

**Competing interests** The authors declare no competing interests.

## References

1. Uhlmann E, Piltz S, Doll U (2005) Machining of micro/minature dies and moulds by electrical discharge machining - recent development. *J Mater Process Technol* 167(2-3):488–493. <https://doi.org/10.1016/j.jmatprotec.2005.06.013>
2. Boswell B, Islam MN, Davies IJ (2018) A review of micro-mechanical cutting. *Int J Adv Manuf Technol* 94(1-4):789–806. <https://doi.org/10.1007/s00170-017-0912-y>
3. Camara MA, Campos Rubio JC, Abrao AM et al (2012) State of the art on micromilling of materials, a review. *J Mater Sci Technol* 28(8):673–685

4. Liang C, Wang F, Huo Z et al (2019) A 2-DOF monolithic compliant rotation platform driven by piezoelectric actuators. *IEEE Trans Ind Electron* 67(8):6963–6974
5. Miao JC, Chen GL, Lai XM, Li HT, Li CF (2007) Review of dynamic issues in micro-end-milling. *Int J Adv Manuf Technol* 31(9):897–904. <https://doi.org/10.1007/s00170-005-0276-6>
6. Altintas Y, Jin X (2011) Mechanics of micro-milling with round edge tools. *CIRP Ann* 60(1):77–80. <https://doi.org/10.1016/j.cirp.2011.03.084>
7. Zhang XW, Ehmann KF, Yu TB et al (2016) Cutting forces in micro-end-milling processes. *Int J Mach Tool Manu* 107:21–40. <https://doi.org/10.1016/j.ijmactools.2016.04.012>
8. Tansel I, Rodriguez O, Trujillo M, Paz E, Li W (1998) Micro-end-milling - I. Wear and breakage. *Int J Mach Tool Manu* 38(12):1419–1436. [https://doi.org/10.1016/s0890-6955\(98\)00015-7](https://doi.org/10.1016/s0890-6955(98)00015-7)
9. Bao WY, Tansel IN (2000) Modeling micro-end-milling operations. Part I: analytical cutting force model. *Int J Mach Tool Manu* 40(15):2155–2173. [https://doi.org/10.1016/s0890-6955\(00\)00054-7](https://doi.org/10.1016/s0890-6955(00)00054-7)
10. Bao WY, Tansel IN (2000) Modeling micro-end-milling operations. Part II: tool run-out. *Int J Mach Tool Manu* 40(15):2175–2192. [https://doi.org/10.1016/s0890-6955\(00\)00055-9](https://doi.org/10.1016/s0890-6955(00)00055-9)
11. Li HZ, Liu K, Li XP (2001) A new method for determining the undeformed chip thickness in milling. *J Mater Process Technol* 113(1-3):378–384. [https://doi.org/10.1016/s0924-0136\(01\)00586-6](https://doi.org/10.1016/s0924-0136(01)00586-6)
12. Dow TA, Miller EL, Garrard K (2004) Tool force and deflection compensation for small milling tools. *Precision Eng J Int Soc Prec Eng Nanotechnol* 28(1):31–45. [https://doi.org/10.1016/s0141-6359\(03\)00072-2](https://doi.org/10.1016/s0141-6359(03)00072-2)
13. Vogler MP, Kapoor SG, Devor RE (2004) On the modeling and analysis of machining performance in micro-endmilling. Part II: Cutting force prediction. *J Manuf Sci Eng Trans Asme* 126(4):695–705. <https://doi.org/10.1115/1.1813471>
14. Bissacco G, Hansen HN, Slunsky J (2008) Modelling the cutting edge radius size effect for force prediction in micro milling. *Cirp Annals-Manuf Technol* 57(1):113–116. <https://doi.org/10.1016/j.cirp.2008.03.085>
15. Lai X, Li H, Li C, Lin Z, Ni J (2008) Modelling and analysis of micro scale milling considering size effect, micro cutter edge radius and minimum chip thickness. *Int J Mach Tool Manu* 48(1):1–14. <https://doi.org/10.1016/j.ijmactools.2007.08.011>
16. Malekian M, Park SS, Jun MBC (2009) Modeling of dynamic micro-milling cutting forces. *Int J Mach Tool Manu* 49(7-8):586–598. <https://doi.org/10.1016/j.ijmactools.2009.02.006>
17. Jin X, Altintas Y (2012) Prediction of micro-milling forces with finite element method. *J Mater Process Technol* 212(3):542–552
18. Jing X, Li H, Wang J, Tian Y (2014) Modelling the cutting forces in micro-end-milling using a hybrid approach. *Int J Adv Manuf Technol* 73(9-12):1647–1656. <https://doi.org/10.1007/s00170-014-5953-x>
19. De Oliveira FB, Rodrigues AR, Coelho RT et al (2015) Size effect and minimum chip thickness in micromilling. *Int J Mach Tool Manu* 89:39–54. <https://doi.org/10.1016/j.ijmactools.2014.11.001>
20. Grossi N, Sallese L, Scippa A, Campatelli G (2015) Speed-varying cutting force coefficient identification in milling. *Precision Eng J Int Soc Prec Eng Nanotechnol* 42:321–334. <https://doi.org/10.1016/j.precisioneng.2015.04.006>
21. Mamedov A, Layegh KSE, Lazoglu I (2015) Instantaneous tool deflection model for micro milling. *Int J Adv Manuf Technol* 79(5-8):769–777. <https://doi.org/10.1007/s00170-015-6877-9>
22. Thepsonthi T, Ozel T (2015) 3-D finite element process simulation of micro-end milling Ti-6Al-4V titanium alloy: experimental validations on chip flow and tool wear. *J Mater Process Technol* 221:128–145. <https://doi.org/10.1016/j.jmatprotec.2015.02.019>
23. Zhang X, Yu T, Wang W (2017) Instantaneous uncut chip thickness modeling for micro-end milling process. *Mach Sci Technol* 21(4):582–602. <https://doi.org/10.1080/10910344.2017.1336181>
24. Yuan Y, Jing X, Ehmann KF, Cao J, Li H, Zhang D (2018) Modeling of cutting forces in micro end-milling. *J Manuf Process* 31:844–858. <https://doi.org/10.1016/j.jmapro.2018.01.012>
25. Jing X, Li H, Wang J, Tian Y (2014) Modelling the cutting forces in micro-end-milling using a hybrid approach. *Int J Adv Manuf Technol* 73(9-12):1647–1656
26. Zhou Y, Tian Y, Jing X, Ehmann KF (2017) A novel instantaneous uncut chip thickness model for mechanistic cutting force model in micro-end-milling. *Int J Adv Manuf Technol* 93(5-8):2305–2319. <https://doi.org/10.1007/s00170-017-0638-x>
27. Zhang X, Yu T, Wang W (2019) Cutting forces modeling for micro flat end milling by considering tool run-out and bottom edge cutting effect. *Proc Inst Mech Eng B J Eng Manuf* 233(2):470–485. <https://doi.org/10.1177/0954405417726811>
28. Armarego E (1998) A generic mechanics of cutting approach to predictive technological performance modeling of the wide spectrum of machining operations. *Mach Sci Technol* 2(2):191–211
29. Jing X, Tian Y, Yuan Y, Wang F (2017) A runout measuring method using modeling and simulation cutting force in micro end-milling. *Int J Adv Manuf Technol* 91(9):4191–4201
30. Mittal RK, Kulkarni SS, Singh RK (2017) Effect of lubrication on machining response and dynamic instability in high-speed micromilling of Ti-6Al-4V. *J Manuf Process* 28:413–421. <https://doi.org/10.1016/j.jmapro.2017.04.007>
31. Wojciechowski S, Matuszak M, Powalka B et al (2019) Prediction of cutting forces during micro end milling considering chip thickness accumulation. *Int J Mach Tool Manu* 147:103466. <https://doi.org/10.1016/j.ijmactools.2019.103466>

**Publisher's note** Springer Nature remains neutral with regard to jurisdictional claims in published maps and institutional affiliations.